



Primate brain pattern-based automated Alzheimer's disease detection model using EEG signals

Sengul Dogan¹ · Mehmet Baygin² · Burak Tasci³ · Hui Wen Loh⁴ · Prabal D. Barua^{5,6} · Turker Tuncer¹ · Ru-San Tan^{7,8} · U. Rajendra Acharya^{9,10,11}

Received: 14 April 2022 / Revised: 8 July 2022 / Accepted: 18 July 2022 / Published online: 12 August 2022
© The Author(s), under exclusive licence to Springer Nature B.V. 2022

Abstract

Electroencephalography (EEG) may detect early changes in Alzheimer's disease (AD), a debilitating progressive neurodegenerative disease. We have developed an automated AD detection model using a novel directed graph for local texture feature extraction with EEG signals. The proposed graph was created from a topological map of the macroscopic connectome, i.e., neuronal pathways linking anatomo-functional brain segments involved in visual object recognition and motor response in the primate brain. This primate brain pattern (PBP)-based model was tested on a public AD EEG signal dataset. The dataset comprised 16-channel EEG signal recordings of 12 AD patients and 11 healthy controls. While PBP could generate 448 low-level features per one-dimensional EEG signal, combining it with tunable q-factor wavelet transform created a multilevel feature extractor (which mimicked deep models) to generate 8,512 ($= 448 \times 19$) features per signal input. Iterative neighborhood component analysis was used to choose the most discriminative features (the number of optimal features varied among the individual EEG channels) to feed to a weighted k-nearest neighbor (KNN) classifier for binary classification into AD vs. healthy using both leave-one subject-out (LOSO) and tenfold cross-validations. Iterative majority voting was used to compute subject-level general performance results from the individual channel classification outputs. Channel-wise, as well as subject-level general results demonstrated exemplary performance. In addition, the model attained 100% and 92.01% accuracy for AD vs. healthy classification using the KNN classifier with tenfold and LOSO cross-validations, respectively. Our developed multilevel PBP-based model extracted discriminative features from EEG signals and paved the way for further development of models inspired by the brain connectome.

Keywords Primate brain modelling · Feature engineering · EEG signal classification · Feature extraction · AD detection

Introduction

Fifty-five million people worldwide currently have dementia, which will reach seventy-eight million in 2030 due to rapidly aging national populations. Dementia ranks as the seventh leading cause of death globally, and Alzheimer's disease (AD) accounts for 60 to 70% of dementia cases (WHO Accessed on 7 Febr 2022). AD is a debilitating neurodegenerative disorder that causes memory loss and cognitive decline due to atrophy and subsequent death of brain cells (Cassani et al. 2018; Mattson 2004). Many AD patients first present with mild symptoms, which then progressively worsen. The diagnosis is based on a formal

evaluation of cognitive function, neuropsychiatric tests, and interviews with the patient and family. Imaging methods and laboratory tests are routinely ordered to exclude other organic causes of impaired mental state (Falk et al. 2012; Houmani et al. 2018; Isik 2010; McBride et al. 2013), which may be amenable to more definitive intervention. Although not included in the standard clinical workup of AD, early subtle and later more overt abnormalities (e.g., slow waves) can often be seen on electroencephalography (EEG) at initial presentation and advanced stages of AD, respectively. While not pathognomonic, these EEG changes serve as corroborative evidence of perturbed cortical activity. A completely normal EEG would give the clinician pause to reconsider the diagnosis of AD.

Extended author information available on the last page of the article

EEG signals, both resting and event-related potentials, are frequently studied in neuroscience research. Visual interpretation of the EEG signal in AD is manually intensive and requires expertise. Notwithstanding this, subtle abnormalities may still be missed, and considerable intra- and inter-observer variability exist. These limitations may be addressed using artificial intelligence methods, which can be harnessed to facilitate the objective classification of EEG signal abnormalities. Poil et al. (2013) studied EEG signals from 61 and 25 patients with mild cognitive impairment (MCI) and AD, respectively. MCI is a transition state between normal and dementia that is of diagnostic and prognostic significance, albeit not all MCI necessarily progress to dementia. Using logistic regression, the authors could predict the conversion from MCI to AD over two years with 88.00% sensitivity and 82.00% specificity. McBride et al. (2014) developed an early AD detection method based on support vector machines (SVM) that attained 79.2% accuracy for three-class classification into MCI, AD, and normal using EEG signals. Kashefpoor et al. (2016) trained their neuro-fuzzy system- and k-nearest neighbor (KNN) classifier-based detection model on the EEG signals of 16 healthy subjects and 11 MCI patients and achieved 88.89% accuracy for detection of MCI. Ruiz-Gómez et al. (2018) used an optimal feature set based on spectral and nonlinear analyses to study the EEG signals of 37 AD, 37 MCI, and 37 controls and compared three classifiers: linear discriminant analysis (LDA), quadratic discriminant analysis (QDA) and multi-layer perceptron artificial neural network (MLP). The best classifier was MLP, which yielded 76.47% classification accuracy for AD versus all other cases. Khatun et al. (2019) extracted 590 features from speech-evoked brain potentials on single-channel EEG signals of 8 MCI patients and 15 healthy controls. Sensitivity, specificity, and F-scores of 87.9%, 84.8%, and 95.0%, respectively, for detection of MCI, were obtained using SVM with radial basis kernel. Yin et al. (2019) proposed a three-dimensional evaluation algorithm for detecting MCI and attained 96.94% classification accuracy with SVM on a dataset comprising 11 MCI patients and 11 healthy controls. Sharma et al. (2020) recorded continuous EEG signals of 16 dementia, 16 early dementia, and 15 healthy subjects during finger tapping and continuous performance tests. They obtained 92.00% model accuracy for detection of early dementia using tenfold cross-validation (CV). Sridhar and Manian (2020) developed a deep bidirectional long short-term memory network to study event-related potentials on EEG signals among healthy controls aged 20–40, 40–60, and > 60 years and MCI patients during auditory and olfactory stimuli as well as imagined and conducted arm movements. Accuracy rates for detecting MCI peaked at 91.93% in the 40–60 age group and declined to 69.53% in the > 60 age

group. Siuly et al. (2020) proposed a method comprising noise removal, segmentation, piecewise aggregate approximation data compression, feature extraction, and classification. They reported 98.78% accuracy for detecting MCI using extreme learning machine classification on their dataset of 11 MCI patients and 16 healthy controls. Huggins et al. (2021) applied AlexNet deep learning model to study 52 AD, 37 MCI and 52 healthy age-matched subjects, where the individuals' EEG signals were combined into tiled topographical maps according to scalp electrode positions. From training the obtained 16,197 topographic images, the model attained an average accuracy of $98.9\% \pm 0.4\%$ for three-class classification into AD, MCI versus healthy aging. These papers illustrate that EEG has been frequently used to research AD and MCI, with the latter receiving more attention. Hence, this study is interested in distinguishing AD from the healthy controls. However, this study has high computational complexity and lower accuracy than our study.

EEG is arguably more sensitive than formal neuropsychiatric testing and clinical evaluation for detecting early cortical dysfunction associated with MCI and AD. However, signal outputs from individual sessions of continuous EEG recordings are voluminous and onerous to interpret manually. Automated artificial intelligence-enabled methods can improve the efficiency of high-throughput screening and, by reducing human bias, the objectiveness of the classification (Bargshady et al. 2022; Kabir et al. 2022; Squires et al. 2022; Tuncer et al. 2022). In this work, we proposed an automated AD detection machine learning model based on the recorded 16-channel EEG signals in the dataset. We created a new graph-based local texture feature extractor named primate brain pattern (PBP) based on a simplified map of the neuronal pathways involved in visual recognition and motor response in the primate brain (see Sect. 3). While the PBP could extract histogram-based low-level features, tunable Q-factor wavelet transform (TQWT) (Selesnick 2011) was employed in parallel to create subbands to generate features at a high level. The PBP-based machine learning model mimicked deep learning models by extracting features at different levels. Iterative neighborhood component analysis (INCA) (Tuncer et al. 2020) was deployed to select the top features to create the final feature vector for each EEG signal channel, and the KNN (Peterson 2009) classifier to calculate the results using both tenfold and leave-one-subject-out (LOSO) CV strategies. Finally, iterative majority voting (IMV) was used to compute a subject-level general result from the 16 results generated (one for each channel of EEG signal) per subject in the dataset. The research gaps identified within the scope of this study and the main contributions are as follows:

Research gaps are given below:

- The accuracy reported for AD and healthy control group classification in the literature is relatively low (Kashefpoor et al. 2016; McBride et al. 2014; Ruiz-Gómez et al. 2018).
- Few studies in the literature have high computational complexity (Huggins et al. 2021; Sridhar and Manian 2020).
- Studies generally used hold-out and k-fold CV strategies (Sharma et al. 2020; Siuly et al. 2020; Yin et al. 2019). Leave-one-subject-out (LOSO) CV has reported low accuracy in one study (Khatun et al. 2019).

Our contributions are given below:

- We present a new local texture feature extractor that uses a directed graph to represent the complex hierarchical pathways that underpin the workings of visual object recognition and motor response in the primate brain.
- The handcrafted AD classification machine learning model possesses linear complexity and is computationally lightweight compared with deep learning models, which have exponential complexity and require millions of parameters to be optimized.
- We fed the PBP-based features extracted from individual EEG signal channels to a shallow weighted KNN classifier. Finally, we used IMV to compute general results from all classification outputs at the subject level.
- We obtained good subject-level classification accuracies of 100% and 92.01% with tenfold and LOSO CV strategies, respectively. While a tenfold CV is an established standard validation model, LOSO CV may be better at simulating real-world classification results of unseen data in models involving analysis of scalp electrode EEG signals (Kunjan et al. 2021).

Material and methods

Materials

The dataset comprised 16-channel EEG signals acquired from 12 AD patients recruited from the Alzheimer's Patients' Relatives Association of Valladolid, as well as 11 healthy controls (Table 1). Folstein's brief mental state examination (MMSE) was used to determine the severity of dementia in AD patients. The maximum MMSE score is determined as 30 in the literature. In addition, 20–24 is called mild dementia, 13–20 is moderate dementia, and 12 and below is severe dementia. Table 1 shows that the average MMSE score is 13.1, indicating that dementia is

moderate. However, five AD patients had an MMSE score of less than 12, suggesting severe dementia.

The EEG signals were recorded in accordance with the international 10–20 system using Profile Study Room 2.3.411 EEG equipment (Smith et al. 2017) (<https://doi.org/10.1088/0967-3334/27/11/004>). The subjects were told to close their eyes and be relaxed for more than 5 min while their EEG signals were recorded at a sampling frequency of 256 Hz. Subsequently, a professional physician evaluated the recorded EEG data to pick the data with the least movement, electromyographic activity, or electrooculographic artefacts. This dataset is available online at Open Science Framework (<https://doi.org/10.17605/OSF.IO/JBYSN>).

Primate brain pattern (PBP)

The connectome depicts the complex neuronal wirings within the brain, which can be at different spatial scales ranging from microscopic cellular resolutions to macroscopic anatomical segments, to facilitate understanding of its inner workings (Kruger et al. 2012). Figure 1 shows a topological map of the neuronal pathways linking anatomo-functional segments (grouped by colors) of the primate brain involved in visual object recognition and motor response: retina (yellow), visual cortex (blue), ventral areas for memory, and non-motor functions (red), and dorsal areas for balance and movement (green). By overlaying the pathways on a grid, we obtained a directed graph, i.e., PBP, where the vertices denoted the key anatomo-functional brain segments and the directed edges, the interlinking neuronal connections (Fig. 2).

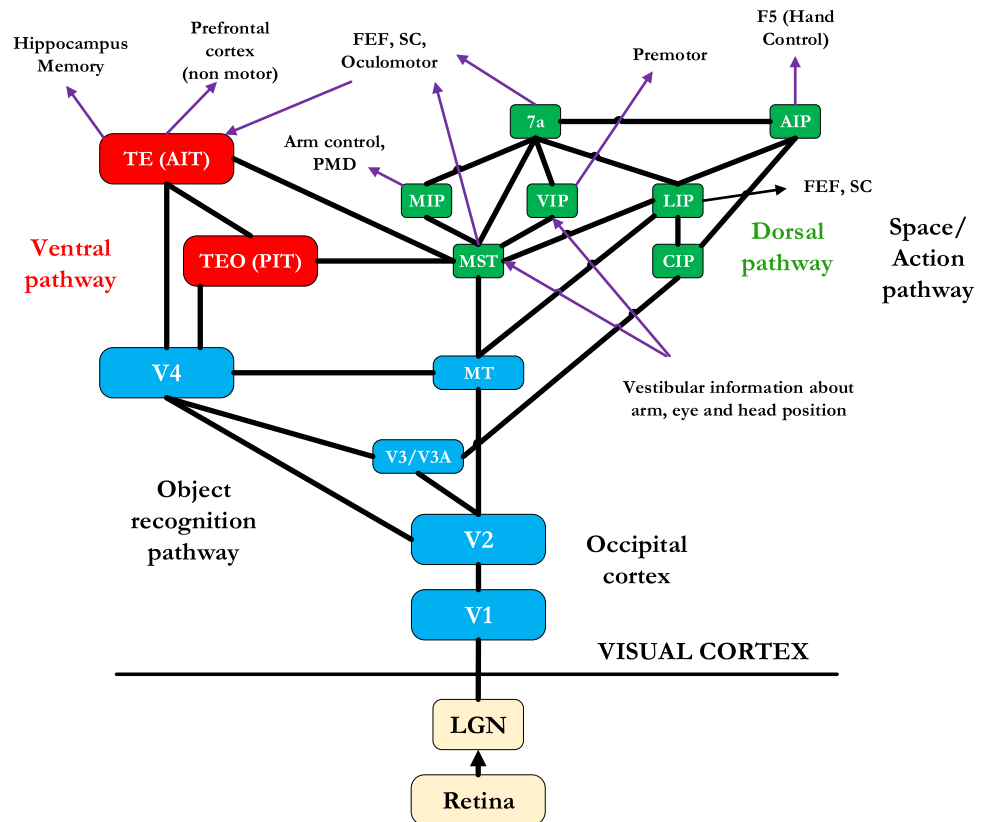
We deployed PBP as a novel graph-based local texture feature extractor in our model. Brain segments (nodes) and neuronal connections (lines) were used to obtain the topological map given in Fig. 2. The numbered arrows represent neuronal connections in Fig. 2 (For example, 1 from Retina to LGN, 2 from LGN to V1, etc.). As shown in Fig. 2, the initial and final locations of each of the 27 arrows in the PBP defined the first and second parameters of the signum function, respectively. Each arrow represents one bit. In this way, a 27-bit long binary sequence is obtained. The 27-bit sequence was calculated using the signum function (Eq. 2). However, it is quite difficult to calculate the decimal equivalent of a 27-bit array. Therefore, the 27-bit string is divided into 7, 7, 7, and 6-bit strings. After that, the feature matrix was calculated using these 4 blocks. The 27 bits thus created were then used to generate 448 features ($2^7, 2^7, 2^7$ and 2^6). The steps are detailed below:

1. Create an overlapping block with a length of 70.

Table 1 Summary of subject information in the dataset created by Alzheimer’s Patients’ Relatives Association of Valladoli

	AD	HC
Number of subjects	12 (5 men, 7 women)	11 (7 men, 4 women)
Age	72.8 ± 8.0 years	72.8 ± 6.1 years
MMSE score	13.1 ± 5.9	30
EEG channels	F3, F4, F7, F8, Fp1, Fp2, T3, T4, T5, T6, C3, C4, P3, P4, O1, O2, Fz, Cz and Pz	

Fig. 1 Topological map of anatomo-functional brain segments (nodes) and neuronal connections (thin black lines) involved in visual recognition and motor response (Kruger et al. 2012). The nodes have been labelled as follows: LGN lateral geniculate nucleus; VI-V4 visual cortices; PIT: posterior inferotemporal area; AIP anterior intraparietal sulcus; LIP lateral intraparietal sulcus; VIP ventral intraparietal sulcus; MIP medial intraparietal sulcus; CIP central intraparietal sulcus; MT middle temporal visual area; MST middle temporal crescent; 7a: posterior half of area; AIT anterior inferotemporal cortex; FEF frontal eye field; SC striate cortex; F5 motor planning execution; PMD dorsal premotor area



$$ob(j) = signal(i + j - 1), i \in \{1, 2, \dots, len - 69\}, i \in \{1, 2, \dots, 70\} \quad (1)$$

where ob is the overlapping block with a length 70; $signal$, the EEG signal; and len , the length of $signal$.

2. Transform the created ob to 10×7 sized matrices (m) to apply our proposed pattern.
3. Extract binary features by deploying sigum function and the corresponding parameters (see Fig. 2).

$$sig(f, s) = \begin{cases} 0, & f - s < 0 \\ 1, & f - s \geq 0 \end{cases} \quad (2)$$

where $sig(\dots)$ represents the sigum function; and f and s , the first and second parameters, respectively. The binary feature extraction process of the proposed model is tabulated in Table 2.

The sequence of the bit generation process is

tabulated in Table 2. Herein, the “No” column shows the numbered graph in Fig. 2, while the “Equation” column shows the cells in Fig. 2. For example, No-1 in Table 2 represents transition-1 from cell (10,4) to cell (9,4). Another example, No-27 in Table 2 denotes transition-27 from cell (4,6) to cell (1,7). In this way, the sigum function is applied to the EEG signal values in the cells thanks to the mapping technique.

4. Generate four map signals from the extracted bits.

$$map^1(i) = \sum_{j=1}^7 bit(j) \times 2^{j-1} \quad (3)$$

$$map^2(i) = \sum_{j=1}^7 bit(j + 7) \times 2^{j-1} \quad (4)$$

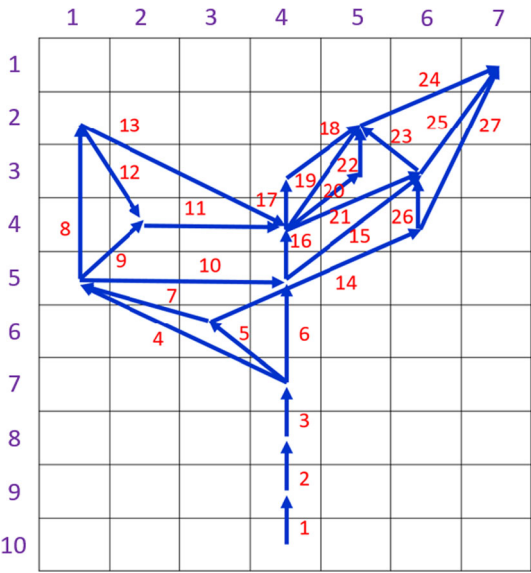


Fig. 2 Primate brain pattern with 27 directed edges created by overlaying the topological map of the brain network in Fig. 1 on a grid

Table 2 Sequential extraction of 27 bits using sigum function with hyperparameters corresponding to the initial and final spatial positions of each directed edge of the primate brain pattern

No	Equation	No	Equation	No	Equation
1	$sig(m(10, 4), m(9, 4))$	10	$sig(m(5, 1), m(5, 4))$	19	$sig(m(4, 4), m(2, 5))$
2	$sig(m(9, 4), m(8, 4))$	11	$sig(m(4, 2), m(4, 4))$	20	$sig(m(4, 4), m(3, 5))$
3	$sig(m(8, 4), m(7, 4))$	12	$sig(m(2, 1), m(4, 2))$	21	$sig(m(4, 4), m(3, 6))$
4	$sig(m(7, 4), m(5, 1))$	13	$sig(m(2, 1), m(4, 4))$	22	$sig(m(3, 5), m(2, 5))$
5	$sig(m(7, 4), m(6, 3))$	14	$sig(m(6, 3), m(4, 6))$	23	$sig(m(3, 6), m(2, 5))$
6	$sig(m(7, 4), m(5, 4))$	15	$sig(m(5, 4), m(3, 6))$	24	$sig(m(2, 5), m(1, 7))$
7	$sig(m(6, 3), m(5, 1))$	16	$sig(m(5, 4), m(4, 4))$	25	$sig(m(3, 6), m(1, 7))$
8	$sig(m(5, 1), m(2, 1))$	17	$sig(m(4, 4), m(3, 4))$	26	$sig(m(4, 6), m(3, 6))$
9	$sig(m(5, 1), m(4, 2))$	18	$sig(m(3, 4), m(2, 5))$	27	$sig(m(4, 6), m(1, 7))$

$$map^3(i) = \sum_{j=1}^7 bit(j + 14) \times 2^{j-1} \tag{5}$$

$$map^4(i) = \sum_{j=1}^6 bit(j + 21) \times 2^{j-1} \tag{6}$$

where map^1 , map^2 , map^3 and map^4 are the map signals generated from the first, second, third, and fourth-bit groups. These maps are coded with 7,7,7 and 6 bits, respectively.

- Extract four histograms from the four map signal created. These histograms are named h^1 , h^2 , h^3 and h^4 . The maximum number of patterns that can be obtained using 7 bits is 128. A similar situation is 64 for 6 bits. Therefore, the lengths of these histograms are 128

- (= 2^7), 128 (= 2^7), 128 (= 2^7), and 64 (= 2^6), respectively.
- Merge the four histograms into a feature vector with 448 features. $(h^1 + h^2 + h^3 + h^4 = 128 + 128 + 128 + 64)$

Proposed model

The PBP could only extract low-level histogram-based handcrafted features. To overcome this limitation, we combined TQWT and PBP to create a multilevel feature extractor (see Fig. 3), mimicking deep learning models. From each EEG signal, TQWT with high oscillatory parameters (q-factor: 3.5, redundancy value: 4, and the number of levels: 17) was used to create 18 subbands; and PBP to extract 448 features from every subband in addition to the raw EEG signal. All extracted features were concatenated to form a feature vector of length 8,512 (= 448×19). INCA was then applied to the latter vector

to choose the most discriminative features to feed to a shallow KNN classifier for classification using two validation strategies, tenfold CV and LOSO. Finally, IMV was used to compute a single subject-level result from all 16 model classification outputs of the input 16-channels EEG signals.

Step-wise explanation of the process is given below.

Step 1: Apply TQWT to EEG signal to generate subbands.

$$sb = TQWT(signal, 3.5, 4, 17) \tag{7}$$

where $TQWT(.,.,.,.)$ is the TQWT subband calculation function, which requires the input of the signal and parameters, i.e., q-factor, redundancy value, and the number of levels, that the users can assign. In this respect, TQWT is a flexible wavelet transformation. By using TQWT, high-level features have been generated. We have

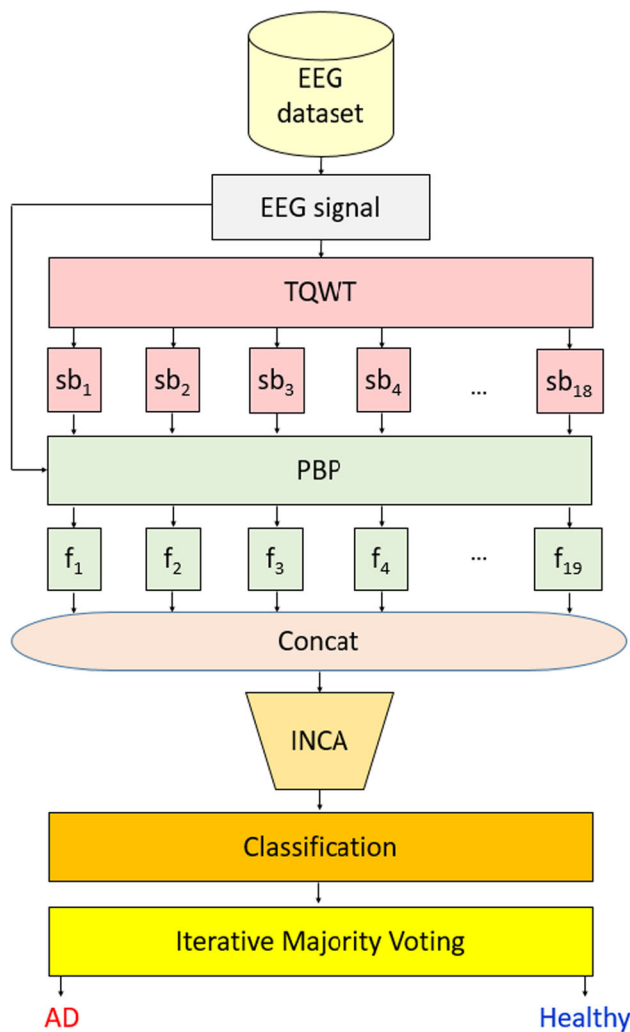


Fig. 3 Illustration of the proposed classification model. *AD* Alzheimer's disease; *Concat*: concatenation; *EEG* electroencephalography; *f* extracted features; *INCA* iterative neighborhood component analysis; *PBP* primate brain pattern; *sb*: subband; *TQWT* tunable Q-factor wavelet transform (TQWT)

used high oscillatory transformations using TQWT since the best performance has been acquired by using these parameters according to the experiments. The used oscillatory and redundancy values were given in the TQWT manual (Selesnick 2011), and the number of levels (*J*) has been calculated using 70 (the length of the used overlapping block for PBP).

Step 2: Extract features from subbands and EEG signals by deploying the PBP function.

$$f_1 = PBP(signal) \quad (8)$$

$$f_{h+1} = PBP(sb_h), h \in \{1, 2, \dots, 18\} \quad (9)$$

Step 3: Create the final feature vector by merging the generated features.

$$X(j + 448 \times (t - 1)) = f_t(j), t \in \{1, 2, \dots, 19\}, j \in \{1, 2, \dots, 448\} \quad (10)$$

Step 4: Choose the most discriminative features by deploying INCA. INCA, developed by Tuncer et al. (2020), is an iterative version of the neighborhood component analysis feature selection function that uses two parameters: loss value generator and range of the features. In this method, the weights of the features are determined by NCA. After that, classification is made starting from the most weighted feature, and reclassification is performed by increasing the number of features in each iteration. At the point where the best classification performance is reached, the optimum number of features is determined but NCA cannot select the optimal feature vector. Therefore, an improved version of the NCA must be used. In this research, INCA feature selector has been used. INCA is a parametric feature selection function. To control the cost of unlimited iterative searching, we define the INCA iteration range in the model as 100 to 1000; i.e., the feature selector will evaluate 901 feature vectors by using this range. Weighted KNN is used here to calculate the misclassification rate of each feature vector, and those with the minimum misclassification rates will be selected as the optimal feature vectors. The dataset has 16 channels, and INCA is applied to each channel. INCA chooses a variable number of features from each channel to determine the optimal feature vector. The number of selected features for each channel is tabulated in Table 3.

The dimensions of the chosen optimal features per the channels are given. These selected optimal feature vectors are then fed to the classifier.

Step 5: Classify the chosen features by deploying KNN with the following attributes:

- k: 10,
- Distance weight: Squared inverse,
- Distance: Euclidean,

Table 3 The number of selected features per channel

No	Number of features	No	Number of features
1	153	9	396
2	120	10	672
3	134	11	103
4	165	12	192
5	107	13	437
6	107	14	834
7	120	15	283
8	210	16	189

These attributes have defined them as weighted KNN classifiers. Two validation techniques were used in this study. These are the tenfold CV and the LOSO CV, respectively. In the tenfold CV method, the entire dataset is divided into ten equal groups, and each group is used in both the test and training phases. In LOSO CV, subject-based grouping is done. In other words, a subject is tested in each iteration. Then, the remaining subjects are used for training.

Step 6: Apply IMV to the calculated results to obtain the general results. The used EEG dataset has 16 channels. By deploying Steps 1–5, channel-wise results are calculated. The calculated 16 prediction vectors are then used to calculate the general results. IMV, developed by Dogan et al. (2021), is used to conduct optimal majority voting. In IMV, prediction vectors and accuracy values of all channels are used. The method calculates a general result using the prediction vectors of the channels with the highest accuracy. A minimum of three channels must be used for majority voting. After that, majority voting is performed in each iteration until the total number of channels is reached. At the last stage of the application, classification accuracies are calculated using voted prediction vectors. The pseudocode of IMV is given below.

processing unit was been used to implement the model.) Standard performance metrics were used to evaluate model classification performance: sensitivity, specificity, and accuracy. The channel-wise results of tenfold and LOSO CV, without IMV, are summarized in Table 4. The best classification accuracy was obtained by deploying a tenfold CV on the 15th channel EEG signal.

The best result for each metric is shown in bold font. The best single-channel classification accuracy rates with tenfold CV (99.40%) and LOSO CV (88.54%) were obtained from the 15th and third EEG signal channels, respectively. Using IMV, the best general classification results with tenfold CV (100% sensitivity, 100% specificity, and 100% accuracy) and LOSO CV (97.25% sensitivity, 84.03% specificity, and 92.01% accuracy) were obtained by using the top 7 and 9 channels, respectively. Confusion matrices of the best-voted results are shown in Fig. 4.

Our combined ML classification model possessed linear time complexity that can be decomposed into four fundamental phases below.

Feature extraction TQWT and PBP were sequentially used to generate feature vectors. TQWT is a multilevel transformation that decreases the signal length at each

Algorithm 1. Iterative majority voting procedure.

<p>Input: Prediction vectors of all channels ($PredVec$) and accuracies (acc) of all channels.</p> <p>Output: The optimal voted result.</p>
<pre> 01: Sort by descending and obtaining qualified indexes (qid). 02: for $h=3$ to 16 do // 16 defines number of channels 03: for $i=1$ to $length(PredVec_h)$ do 04: for $j=1$ to h do 05: $array(j) = PredVec_{qid(j)}(i)$; 06: end for j 07: $PredVecVoted_{h-2}(i) = mode(array)$ // Generate voted prediction vector. 08: end for i 09: end for h 10: Compute classification accuracies using the voted prediction vectors ($PredVecVoted$). 11: Choose the maximum accurate result as an optimal voted result. </pre>

Experiments

The PBP-based EEG classification model was implemented in MATLAB (2021b) environment on a personal computer with Intel® Core™ i9-9900 Processor (16 GB memory, 3.6 GHz) using Microsoft Windows 10.1 Professional operating system. (None of the cores of the graphical

level. PBP is a handcrafted local texture feature extractor with time complexity (PBP) = $O(n)$, where n is the length of the used signal. The time complexity of this stage is $O(n \log n)$.

Feature selection The INCA feature selector uses an iteration and loss value generator. The computation complexity is $O(ilk)$ Where i is the number of iterations; l , the

Table 4 Channel-wise classification results (%) of model using tenfold and leave-one-subject-out cross-validations

Channel	Tenfold CV			Leave-one-subject out CV		
	Sen	Spe	Acc	Sen	Spe	Acc
1	95.25	87.07	92.01	82	79.47	81
2	98.50	85.17	93.21	94.25	64.64	82.50
3	96.25	93.16	95.02	91	84.79	88.54
4	95.25	92.78	94.27	78	69.58	74.66
5	96.75	71.48	86.73	94	56.27	79.03
6	94.75	92.40	93.82	85.75	68.82	79.03
7	98.50	91.25	95.63	77.25	26.62	57.16
8	93.50	58.94	79.79	85.75	33.46	65.01
9	91.25	92.40	91.70	88	76.05	83.26
10	98.50	98.48	98.49	76.50	55.13	68.02
11	97.50	99.24	98.19	87.50	74.90	82.50
12	97.75	93.92	96.23	77.50	56.27	69.08
13	96.75	50.95	78.58	93.50	34.60	70.14
14	97.75	93.54	96.08	80.25	71.86	76.92
15	99.25	99.62	99.40	89.25	48.67	73.15
16	95	98.48	96.38	63.25	58.17	61.24

****AD** Alzheimer's disease; **Acc** accuracy; **CV** cross-validation; **HC** healthy control; **MCI** mild cognitive disorder; **Sen** sensitivity; **Spe** specificity

computational complexity of the used classifier; k , the computational complexity multiplier of the neighborhood component analysis (Goldberger et al. 2004a).

Classification KNN classifier was used both as a loss value calculator in the INCA feature selector and the model's classification method. The time burden of the classification phase is $O(l)$.

Iterative majority voting This is the simplest phase of the classification model. We used an iteration to obtain the maximum voted accuracy. In IMV, the mode function was used to calculate voted results and has a time complexity equal to $O(i)$.

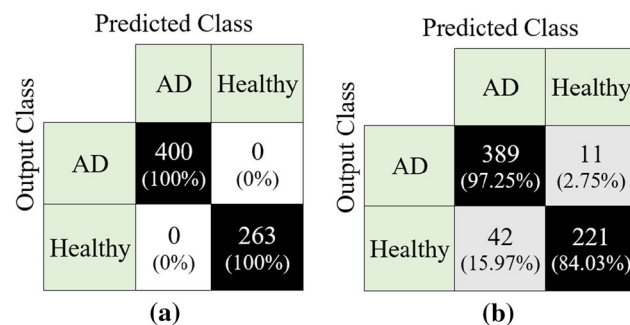


Fig. 4 Confusion matrices of the computed voted results using tenfold cross-validation (a) and leave-one-subject-out cross-validation (b). AD, Alzheimer's disease

In total, the model's time complexity is $O(n \log n + ilk + 1 + i) \cong O(n \log n + ilk)$, which is linear, as mentioned.

Discussion

We have presented a new PBP local feature extractor based on a connectome-inspired directed graph derived from a simplified topological map of the neuronal pathways involved in visual object recognition and motor response in the primate brain. This was combined with TQWT for multilevel texture feature extraction. INCA was applied to choose the most valuable features in each of the 16 EEG signal channels using the KNN classifier as the loss value generator. In this dataset, the number of the features in the optimal feature vectors is selected by INCA for channels (see Table 2). KNN was used to classify the selected features using tenfold and LOSO CV, which yielded 100% and 92.01%, respectively, after IMV of all 16-channel EEG signal classification results. Indeed, these general accuracies rates were numerically higher than the best channel-wise accuracies of 99.40% and 88.54% attained with tenfold and LOSO CV, respectively.

In the model, we chose to use a modified KNN, weighted KNN, as a loss vector calculator during INCA feature selection and as the classifier for binary classification of each EEG signal into AD vs. normal. Before choosing the KNN method, it was tested in other classifiers, and its performances were observed. In the classifier determination phase, the classifiers in the MATLAB (2021b) Classification Learner Toolbox have been tested. The classification performance of the weighted KNN compared favorably against other classifiers (bi-layered ANN (Khan et al. 2022), logistic discriminant (Cinbis et al. 2011), subspace KNN (Xing et al. 2018), weighted KNN (Zuo et al. 2008), kernel Naïve Bayes (Sharma and Mukhopadhyay 2021), logistic regression (Li and Jimenez 2018), cubic SVM (Jain et al. 2018), medium tree (Lamba et al. 2020)) in the MATLAB (2021b) classification learner when deployed with a tenfold CV on the common 15th channel EEG signal (Fig. 5).

As given in Fig. 5, the best classification result was obtained with the kNN algorithm. For this reason, kNN method was used as a loss vector calculator in iterative feature selection and classifier in the study. The classification performance of the presented PBP-based model was also compared against other AD detection models using the same dataset in the literature Table 5. As can be seen, our proposed model attained satisfactory results of over 92% accuracy rates with the two validations model. Of note, the 100% AD classification accuracy achieved using a tenfold CV is the among all studies.

As can be seen from Table 5, the studies performed by Abásolo et al. (2006), Escudero et al. (2006), and Simons et al. (2018) generally make entropy-based calculations. Although these methods have low computational complexity, the achieved accuracy values are low. When other studies using the same dataset were examined, a TQWT-based method was proposed by Puri et al. (2022b). An accuracy value of 96.20% was achieved with this method. This accuracy value is 100% and higher in our study. In addition, empirical mode decomposition and Hjorth parameters are used in another method proposed by Puri et al. (2022a, b, c). In this paper, an accuracy of 92.90% was achieved with the tenfold CV method. In the previous study by the same author (Puri et al. 2022c), spectral entropy and Kolmogorov complexity were used and provided an accuracy of 95.6%. In our study, 100% accuracy was achieved with the tenfold CV method. In addition, the LOSO CV strategy was applied in this study, and an accuracy of 92.01% was obtained in subject-based classification. As seen from the Table, our method produces high accuracy values and LOSO CV results that are important for real-world applications. In addition, the developed model has low computational complexity, making it usable for real-world applications.

The benefits and limitations of the presented PBP-based model are listed.

Benefits:

- A public AD EEG dataset was used in this work. We have chosen to work on AD detection as it is the most commonly seen dementia.

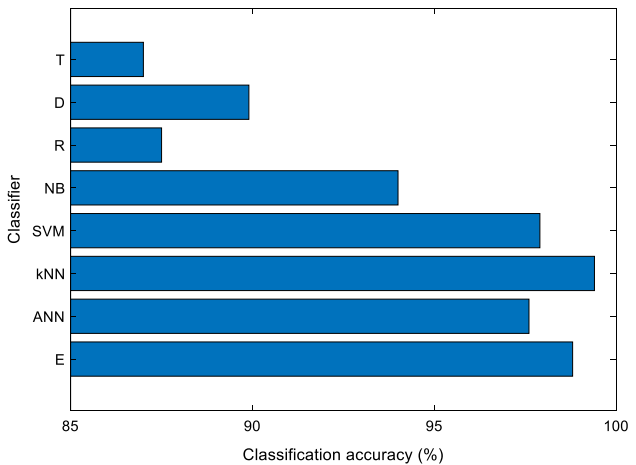


Fig. 5 Comparison of accuracies of different classifiers on the common 15th channel EEG signal using tenfold CV. The classifiers were deployed with default settings. ANN, bi-layered ANN; D, logistic discriminant; E subspace kNN; kNN, weighted kNN; NB, kernel Naïve Bayes (NB); R, logistic regression; SVM, cubic SVM; T, medium tree

Table 5 Comparison of the proposed model with other Alzheimer’s disease detection models using the same dataset in the literature

Study	Year	Method	Split ratio	Results (%)
Abásolo et al. (2006)	2006	Spectral entropy and sample entropy	–	Acc.:77.27 Spe.:90.91 Sen.:63.64 Auc.:83.47
Escudero et al. (2006)	2006	Multiscale entropy	–	Acc.:90.91 Spe.:90.91 Sen.:90.91 Auc.:93.39
Simons et al. (2018)	2018	Fuzzy entropy	–	Acc.:86.36 Sen.:90.91 Spe.:81.82 Auc.:85.95
Puri et al. (2022b)	2022	TQWT, Katz’s fractal dimension, Tsallis entropy, Relyi’s entropy, and kurtosis, ensemble bagged tree	Tenfold CV	Acc: 96.20 Sen.:90.49 Spe.:97.50 Pre.:93.48 FScr.:95.09 Mcc.:87.37
Puri et al. (2022a, b, c)	2022	Empirical mode decomposition and Hjorth parameters using Kruskal–Wallis test, Least Square SVM	Tenfold CV	Acc: 92.90 Sen.:94.32 Spe.:94.34 Pre.:94.33 FScr.:94.32 Auc.:98.93
Puri et al. (2022c)	2022	Spectral Entropy and Kolmogorov Complexity, SVM	Tenfold CV	Acc.:95.6 Pre.:95.2 Rec.:95.2 FScr.:95.1 Auc.:98.3
Our model		Primate brain pattern	1. Tenfold CV 2. LOSO CV	tenfold CV Acc: 100 Sen: 100 Spe: 100 LOSO-CV Acc: 92.01 Sen: 97.25 Spe: 84.03

- The connectome of the primate brain-inspired us to create a novel PBP for handcrafted feature extraction. This was combined with TQWT for multilevel feature generation. INCA was used to choose highly distinctive features that were fed to weighted KNN for classification. Finally, IMV was used to obtain the optimal voted (general) result.

- tenfold and LOSO CV were used to compute channel-wise and general results.
- Our model attained high accuracy for detection of AD vs. healthy control: 92.01% and 100% classification accuracies using LOSO CV and tenfold CV, respectively.
- The model has an undemanding linear computational complexity of $O(n \log n + ilk)$.
- The presented PBP-based model is efficient and straightforward. Therefore, researchers/developers can use this model to solve their classification problems.

Limitations:

- The EEG dataset comprising 663 observations in 23 subjects is relatively modest.
- We used a conventional classifier in our experiments to test the classification capability of the generated features. Hyperparameters of the classifier can be further optimized, or a more powerful classifier can be deployed instead.

This model can be tested on a larger EEG dataset as future works. Similarly, the proposed system could also be evaluated with other neurological diseases such as Parkinson's disease, epilepsy, and stroke. Future work to develop a deep learning model as the classification unit and a cloud system for AD detection is also under consideration. We have used LOSO to better approximate real-world classification results with the model (Kunjan et al. 2021), which provides a more realistic expectation of its performance when deployed for screening AD in the clinic.

Conclusions

We have developed an AD detection model that may be incorporated into automated AD diagnosis systems to help clinicians screen for the disease. The model is computationally lightweight and can be easily implemented on standard hardware. Key elements of the model include multilevel feature extraction, iterative feature selection, classification, and IMV. The model yielded 92.01% and 100% accuracies using LOSO and tenfold CVs, respectively, which attests to its discriminative utility for AD vs. healthy classification. In addition, we are the first to seek inspiration from and have successfully used the primate brain's connectome to develop a machine learning classification model. Hopefully, our experience and results with this connectome-inspired graph-based model will motivate other researchers to experiment with this promising new approach.

Conflict of interest

The authors declare that they have no conflict of interest.

Ethical approval

Ethics approval was not required for this research.

Appendix

Tunable Q-factor wavelet transform (TQWT)

As a representative wavelet transform expressing wavelets in the frequency domain, discrete-time signals of finite length are analyzed using radix-2 FFTs (Selesnick 2011). Compared to traditional Q-fixed wavelet transforms, TQWT has the excellent feature of estimating the Q factor easily and continuously adjusting it depending on the different oscillations of different signals. Moreover, successful error feature generation using TQWT-based parsing relies on appropriate TQWT parameters such as parsing level, Q factor, and redundancy (Kong et al. 2018). As noted, TQWT takes three parameters (Q: oscillatory value, r: redundancy, J: number of level). The first parameter is Q and it assigns number of oscillations. If Q is 1, there is no oscillations.

TQWT contains two filter banks and these two-channel filter banks consist of a low-pass and a high-pass channel. The low-pass channel has a low-pass filter (LPF) followed by a low-pass scaling factor (LCF). The high-pass channel has a high-pass filter (HPF) followed by a high-pass scaling factor (HCF). The ratio of the center frequency (CF) of each subband to the bandwidth is equal to the Q factor used to implement the TQWT. The following expressions can be used to calculate the MF and bandwidth of a subband (Selesnick 2011):

$$CF(J) = (LCF)^J \left[\frac{2 - (HCF)}{4(LCF)} \right] f_s \quad (1)$$

$$\text{Bandwidth}(j) = \frac{(HCF)(LCF)^{J-1}}{4} \quad (2)$$

Equations 1 and 2 define the effect of scaling factors on the center frequency and bandwidth is observed. Herein j represents the subband number where $1 \leq J \leq J + 1$ f_s is the sampling frequency. The Q factor is controlled by R, and its connection is given in Eqs. 3 and 4 (Zhang et al. 2001).

$$LCF = 1 - \frac{HCF}{R} \quad (3)$$

$$HCF = \frac{2}{Q+1} \quad (4)$$

Iterative neighborhood component analysis (INCA)

In order to explain INCA better, we first gave information about NCA in this section. Neighborhood component analysis (NCA) is a technique for reducing dimensions and selecting features. In machine learning applications, it is crucial to measure features. In classification studies, NCA is widely used as one of the most successful learning algorithms. Using NCA, classification operations are carried out by learning the projections of the vectors that optimize the nearest neighbor classifier's accuracy criteria. As another option, the NCA can select a linear projection that optimizes the performance of the nearest neighbor classifier within the projection area (Goldberger et al. 2004a).

NCA is a method that aims to learn the Mahalanobis distance to be used in classification and performs the classification using this distance. While the NCA method calculates Mahalanobis distance, it learns the projection matrix and prevents the inverse operation of the matrix.

This method uses the Mahalanobis distance formula described below to define the Mahalanobis distance.

$$dis(y_i - y_j) = (P^T y_i - P^T y_j)^T (P^T y_i - P^T y_j) \quad (5)$$

In this equation, P is defined as the projection matrix that transforms the data. Thus, NCA moves from learning the Mahalanobis distance to learning the P matrix.

A data in the training data determines the class label by choosing another data as a neighbor. Data with transformed probability values are defined using softmax regression with euclidean distances.

$$p_{ij} = \frac{\exp(-\|P^T y_i - P^T y_j\|^2)}{\sum_{k \neq i} \exp(-\|P^T y_i - P^T y_k\|^2)}, p_{ii} = 0 \quad (6)$$

Based on the stochastic selection rules, the probability of correctly classifying the data is calculated, and the set of data in the same class is displayed.

$$p_i = \sum_j j \in c_i p_{ij} \quad (7)$$

$$C_i = \{ \{ j | z_j = z_i \} \} \quad (8)$$

NCA then calculates the P matrix by maximizing the number of correctly classified points.

$$f(A) = \sum_i p_i = \sum_i i \sum_j j \in c_i p_{ij} \quad (9)$$

The f value that changes according to the P matrix gives rise to the following gradient rule.

$$\frac{\partial f}{\partial A} = 2 \sum_i i (p_i \sum_k k p_{ik} (y_i - y_j)(y_i - y_j)^T \sum_j j \in c_i p_{ij} (y_i - y_j)(y_i - y_j)^T P \quad (10)$$

Thus, a gradient-based optimizer is used.

INCA is an improved version of the NCA feature selector and it is an iterative version of the NCA. The main objective of the INCA feature selector is to choose the optimized number of features. To choose optimal feature vector, we used a loop and loss function. The steps of the INCA are given below.

Step 1 Calculate the qualified indexes by deploying the NCA algorithm.

Step 2 Define a loop range to decrease time complexity.

Step 3 Choose feature vectors iteratively by using the created loop.

Step 4 Apply the used loss function to the selected feature vectors and create a loss array.

Step 5 Select the feature vector with minimum loss value.

kNN

The KNN algorithm is one of the more common algorithms used in general and one of the most widely known and widely used algorithms. Given unlabeled test data, kNN finds the closest k in the data set and then assigns the most appropriate label (Guo et al. 2003).

KNN performs object classification according to the closest training examples. A majority vote of its neighbors classifies an object.

Two situations should be considered in the kNN algorithm. The first of these is the correct choice of k , which affects performance. When k values are large, it may ignore small but important patterns. The other case is to calculate the distance between test samples and neighbors (Zhang 2016). The most popular measure of distance in distance functions are euclidean, manhattan, and Minkowski.

X_1, X_2, \dots, X_n and Y_1, Y_2, \dots, Y_n represent the feature vector where n is the dimension of the feature space. The mathematical representation of the Euclidean distance is given in Eq. 11.

$$dis_{euclidean}(X, Y) = \sqrt{\sum_{i=1}^n (X_i - Y_i)^2} \quad (11)$$

The mathematical representation of the manhattan distance, which calculates the difference of two data points in absolute value, is given in Eq. 12.

$$dis_{manhattan}(X, Y) = \sum_{i=1}^n |(X_i - Y_i)| \quad (12)$$

The mathematical representation of the Minkowski distance, where $p \in (0, \infty)$ for a constant p , is given in Eq. 13.

$$dis_{minkowski}(X, Y) = \left(\sum_{i=1}^n |X_i - Y_i|^p \right)^{1/p} \quad (13)$$

Mode-based majority voting

Majority voting relies on the principle of normalization, which is derived from the sum of the probabilities given by the classifiers. As a result of this classification, the highest probability class combination result is obtained within the normalized result (Suen and Lam 2000).

Author contributions All authors contributed equally to the study.

Funding The authors state that this work has not received any funding.

Data availability Data and relevant material are available from the Datashare website: <http://datashare.is.ed.ac.uk/handle/10283/2783> (Smith et al. 2017).


References

- Abásolo D, Hornero R, Espino P, Alvarez D, Poza J (2006) Entropy analysis of the EEG background activity in Alzheimer's disease patients. *Physiol Meas* 27:241
- Bargshady G, Zhou X, Barua PD, Gururajan R, Li Y, Acharya UR (2022) Application of CycleGAN and transfer learning techniques for automated detection of COVID-19 using X-ray images. *Pattern Recognit Lett* 153:67–74
- Cassani R, Estarellas M, San-Martin R, Fraga FJ, Falk TH (2018) Systematic review on resting-state EEG for Alzheimer's disease diagnosis and progression assessment. *Disease Mark* 2018
- Cinbis RG, Verbeek J, Schmid C (2011) Unsupervised metric learning for face identification in TV video. In: 2011 international conference on computer vision, Barcelona, 2011. IEEE, pp 1559–1566
- Dogan A et al (2021) PrimePatNet87: Prime pattern and tunable q-factor wavelet transform techniques for automated accurate EEG emotion recognition. *Comput Biol Med* 138:104867
- Escudero J, Abásolo D, Hornero R, Espino P, López M (2006) Analysis of electroencephalograms in Alzheimer's disease patients with multiscale entropy. *Physiol Meas* 27:1091
- Falk TH, Fraga FJ, Trambaiolli L, Anghinah R (2012) EEG amplitude modulation analysis for semi-automated diagnosis of Alzheimer's disease. *EURASIP J Adv Signal Process* 2012:1–9. <https://doi.org/10.1186/1687-6180-2012-192>
- Goldberger J, Hinton GE, Roweis S, Salakhutdinov RR (2004a) Neighbourhood components analysis. *Adv Neural Inf Process Syst* 17:513–520
- Guo G, Wang H, Bell D, Bi Y, Greer K KNN model-based approach in classification. In: OTM confederated international conferences“ on the move to meaningful internet systems”, 2003. Springer, pp 986–996
- Houmani N, Vialatte F, Gallego-Jutglà E, Dreyfus G, Nguyen-Michel V-H, Mariani J, Kinugawa K (2018) Diagnosis of Alzheimer's disease with electroencephalography in a differential framework. *PLoS ONE* 13:e0193607
- Huggins CJ et al (2021) Deep learning of resting-state electroencephalogram signals for three-class classification of Alzheimer's disease, mild cognitive impairment and healthy ageing. *J Neural Eng* 18:046087
- Isik AT (2010) Late onset Alzheimer's disease in older people. *Clin Interv Aging* 5:307
- Jain U, Nathani K, Ruban N, Raj ANJ, Zhuang Z, Mahesh VG Cubic SVM classifier based feature extraction and emotion detection from speech signals. In: 2018 international conference on sensor networks and signal processing (SNSP), 2018. IEEE, pp 386–391
- Kabir HD, Khanam S, Khozeimeh F, Khosravi A, Mondal SK, Nahavandi S, Acharya UR (2022) Aleatory-aware deep uncertainty quantification for transfer learning. *Comput Biol Med* 143:105246
- Kashefpoor M, Rabbani H, Barekatin M (2016) Automatic diagnosis of mild cognitive impairment using electroencephalogram spectral features. *J Med Signals Sens* 6:25
- Khan MU et al (2022) Artificial neural network-based cardiovascular disease prediction using spectral features. *Comput Electr Eng* 101:108094
- Khatun S, Morshed BI, Bidelman GM (2019) A single-channel EEG-based approach to detect mild cognitive impairment via speech-evoked brain responses. *IEEE Trans Neural Syst Rehabil Eng* 27:1063–1070
- Kong Y, Wang T, Chu F (2018) Adaptive TQWT filter based feature extraction method and its application to detection of repetitive transients. *Sci China Technol Sci* 61:1556–1574
- Kruger N et al (2012) Deep hierarchies in the primate visual cortex: What can we learn for computer vision? *IEEE Trans Pattern Anal Mach Intell* 35:1847–1871
- Kunjan S et al (2021) The necessity of leave one subject out (LOSO) cross validation for EEG disease diagnosis. *International conference on brain informatics*. Springer, pp 558–567
- Lamba PS, Virmani D, Castillo O (2020) Multimodal human eye blink recognition method using feature level fusion for exigency detection. *Soft Comput* 24:16829–16845
- Li N, Jimenez R (2018) A logistic regression classifier for long-term probabilistic prediction of rock burst hazard. *Nat Hazards* 90:197–215
- Mattson MP (2004) Pathways towards and away from Alzheimer's disease. *Nature* 430:631–639
- McBride J, Zhao X, Munro N, Smith C, Jicha G, Jiang Y (2013) Resting EEG discrimination of early stage Alzheimer's disease from normal aging using inter-channel coherence network graphs. *Ann Biomed Eng* 41:1233–1242
- McBride JC et al (2014) Spectral and complexity analysis of scalp EEG characteristics for mild cognitive impairment and early Alzheimer's disease. *Comput Methods Programs Biomed* 114:153–163
- Peterson LE (2009) K-nearest neighbor. *Scholarpedia* 4:1883
- Poel S-S, De Haan W, van der Flier WM, Mansvelder HD, Scheltens P, Linkenkaer-Hansen K (2013) Integrative EEG biomarkers predict progression to Alzheimer's disease at the MCI stage. *Front Aging Neurosci* 5:58
- Puri D, Nalbalwar S, Nandgaonkar A, Kachare P, Rajput J, Wagh A, (2022a) Alzheimer's disease detection using empirical mode decomposition and Hjorth parameters of EEG signal. *IEEE*, pp 23–28
- Puri D, Nalbalwar S, Nandgaonkar A, Wagh A (2022b) Alzheimer's disease detection from optimal electroencephalogram channels and tunable q-wavelet transform. *Indo Journal of Elec Engg and Comp Sci* 25:1420–1428

- Puri D, Nalbalwar S, Nandgaonkar A, Wagh A (2022c) EEG-based diagnosis of alzheimer's disease using kolmogorov complexity. In: Applied information processing systems. Springer, pp 157–165
- Ruiz-Gómez SJ, Gómez C, Poza J, Gutiérrez-Tobal GC, Tola-Arribas MA, Cano M, Hornero R (2018) Automated multiclass classification of spontaneous EEG activity in Alzheimer's disease and mild cognitive impairment. *Entropy* 20:35
- Selesnick IW (2011) Wavelet transform with tunable Q-factor. *IEEE Trans Signal Process* 59:3560–3575
- Sharma K, Mukhopadhyay A (2021) Kernel naïve Bayes classifier-based cyber-risk assessment and mitigation framework for online gaming platforms. *J Organ Comput Electron Commer* 31:343–363
- Sharma N, Kolekar MH, Jha K (2020) Iterative filtering decomposition based early dementia diagnosis using EEG with cognitive tests. *IEEE Trans Neural Syst Rehabil Eng* 28:1890–1898
- Simons S, Espino P, Abásolo D (2018) Fuzzy entropy analysis of the electroencephalogram in patients with Alzheimer's disease: is the method superior to sample entropy? *Entropy* 20:21
- Siuly S, Alçin ÖF, Kabir E, Şengür A, Wang H, Zhang Y, Whittaker F (2020) A new framework for automatic detection of patients with mild cognitive impairment using resting-state EEG signals. *IEEE Trans Neural Syst Rehabil Eng* 28:1966–1976
- Smith K, Abásolo D, Escudero J (2017) Accounting for the complex hierarchical topology of EEG phase-based functional connectivity in network binarisation. *PLoS ONE* 12:e0186164
- Squires M, Tao X, Elangovan S, Gururajan R, Zhou X, Acharya UR (2022) A novel genetic algorithm based system for the scheduling of medical treatments. *Expert Syst Appl* 195:116464
- Sridhar S, Manian V (2020) Eeg and deep learning based brain cognitive function classification. *Computers* 9:104
- Suen CY, Lam L (2000) Multiple classifier combination methodologies for different output levels. *International workshop on multiple classifier systems*. Springer, pp 52–66
- Tuncer T, Dogan S, Özyurt F, Belhaouari SB, Bensmail H (2020) Novel multi center and threshold ternary pattern based method for disease detection method using voice. *IEEE Access* 8:84532–84540
- Tuncer T, Dogan S, Akbal E, Cicekli A, Rajendra Acharya U (2022) Development of accurate automated language identification model using polymer pattern and tent maximum absolute pooling techniques. *Neural Comput Appl* 34:1–14
- WHO (Accessed on 7 Febr 2022) Dementia, <https://www.who.int/news-room/fact-sheets/detail/dementia>.
- Xing X, Jia X, Meng MQ-H Bleeding detection in wireless capsule endoscopy image video using superpixel-color histogram and a subspace knn classifier. In: 2018 40th annual international conference of the ieee engineering in medicine and biology society (EMBC), 2018. IEEE, pp 1–4
- Yin J, Cao J, Siuly S, Wang H (2019) An integrated MCI detection framework based on spectral-temporal analysis. *Int J Autom Comput* 16:786–799
- Zhang Z (2016) Introduction to machine learning: k-nearest neighbors. *Ann Transl Med* 4:218
- Zhang Y, Wang Y, Wang W, Liu B (2001) Doppler ultrasound signal denoising based on wavelet frames. *IEEE Trans Ultrasonics, Ferroelectr Freq Control* 48:709–716
- Zuo W, Lu W, Wang K, Zhang H Diagnosis of cardiac arrhythmia using kernel difference weighted KNN classifier. In: 2008 computers in cardiology, 2008. IEEE, pp 253–256

Springer Nature or its licensor holds exclusive rights to this article under a publishing agreement with the author(s) or other rightsholder(s); author self-archiving of the accepted manuscript version of this article is solely governed by the terms of such publishing agreement and applicable law.

Authors and Affiliations

Sengul Dogan¹  · Mehmet Baygin² · Burak Tasci³ · Hui Wen Loh⁴ · Prabal D. Barua^{5,6} · Turker Tuncer¹ · Ru-San Tan^{7,8} · U. Rajendra Acharya^{9,10,11}

✉ Sengul Dogan
sdogan@firat.edu.tr

Mehmet Baygin
mehmetbaygin@ardahan.edu.tr

Burak Tasci
btasci@firat.edu.tr

Hui Wen Loh
hwloh002@suss.edu.sg

Prabal D. Barua
prabal.barua@usq.edu.au

Turker Tuncer
turkertuncer@firat.edu.tr

Ru-San Tan
tanrshc@gmail.com

U. Rajendra Acharya
aru@np.edu.sg

¹ Department of Digital Forensics Engineering, College of Technology, Firat University, Elazig, Turkey

² Department of Computer Engineering, College of Engineering, Ardahan University, Ardahan, Turkey

³ Vocational School of Technical Sciences, Firat University, Elazig 23119, Turkey

⁴ School of Science and Technology, Singapore University of Social Sciences, 463 Clementi Road, Singapore 599494, Singapore

⁵ School of Business (Information System), University of Southern Queensland, Toowoomba, QLD 4350, Australia

⁶ Faculty of Engineering and Information Technology, University of Technology Sydney, Sydney, NSW 2007, Australia

⁷ Department of Cardiology, National Heart Centre Singapore, Singapore 169609, Singapore

⁸ Duke-NUS Medical School, Singapore 169857, Singapore

⁹ Department of Electronics and Computer Engineering, Ngee Ann Polytechnic, Singapore 599489, Singapore

¹⁰ Department of Biomedical Engineering, School of Science and Technology, SUSS University, Singapore, Singapore

¹¹ Department of Biomedical Informatics and Medical Engineering, AsiaUniversity, Taichung, Taiwan

Publisher's Note Springer Nature remains neutral with regard to jurisdictional claims in published maps and institutional affiliations.